

● *Original Contribution*

CELL-BASED TWO-REGION COMPETITION ALGORITHM WITH A MAP FRAMEWORK FOR BOUNDARY DELINEATION OF A SERIES OF 2D ULTRASOUND IMAGES

JIE-ZHI CHENG,* CHUNG-MING CHEN,* YI-HONG CHOU,† CURTIS S. K. CHEN,‡
CHUI-MEI TIU,† and KUEI-WU CHEN*

*Institute of Biomedical Engineering, National Taiwan University, Taipei, Taiwan; †Department of Radiology, Taipei Veterans General Hospital and National Yang Ming University, Taipei, Taiwan; and ‡Division of Oral Radiology, Dept. of Oral Medicine, School of Dentistry, University of Washington, Seattle, WA

(Received 10 October 2006, revised 1 April 2007, in final form 26 April 2007)

Abstract—To ensure the delineated boundaries of a series of 2-D images closely following the visually perceivable edges with high boundary coherence between consecutive slices, a cell-based two-region competition algorithm based on a maximum *a posteriori* (MAP) framework is proposed. It deforms the region boundary in a cell-by-cell fashion through a cell-based two-region competition process. The cell-based deformation is guided by a cell-based MAP framework with a posterior function characterizing the distribution of the cell means in each region, the salience and shape complexity of the region boundary and the boundary coherence of the consecutive slices. The proposed algorithm has been validated using 10 series of breast sonograms, including seven compression series and three freehand series. The compression series contains two carcinoma and five fibroadenoma cases and the freehand series contains two carcinoma and one fibroadenoma cases. The results show that >70% of the derived boundaries fall within the span of the manually delineated boundaries. The robustness of the proposed algorithm to the variation of regions-of-interest is confirmed by the Friedman tests and the *p*-values of which are 0.517 and 0.352 for the compression and freehand series groups, respectively. The Pearson's correlations between the lesion sizes derived by the proposed algorithm and those defined by the average manually delineated boundaries are all higher than 0.990. The overlapping and difference ratios between the derived boundaries and the average manually delineated boundaries are mostly higher than 0.90 and lower than 0.13, respectively. For both series groups, all assessments conclude that the boundaries derived by the proposed algorithm be comparable to those delineated manually. Moreover, it is shown that the proposed algorithm is superior to the Chan and Vese level set method based on the paired-sample *t*-tests on the performance indices at a 5% significance level. (E-mail: chung@ntu.edu.tw) © 2007 World Federation for Ultrasound in Medicine & Biology.

Key Words: Boundary delineation, Image series, Maximum *a posteriori*, Cell-based deformation, Two-region competition, EM algorithm.

INTRODUCTION

Segmentation of objects of interest in a series of 2-D images is an essential process for various quantitative ultrasound image analyses. By identifying the object boundaries in a series of 2-D sonograms, higher-level information may be derived and integrated to characterize the functional properties of the objects (Noble and Boukerroui 2006). Typical examples are using 3-D volume and surface irregularity to characterize the malignancy of a breast lesion (Chen et al. 2003), quantitative

analyses based on boundary information of vessel walls and lumens in a series of intravascular ultrasound images (Lee et al. 1995; Nissen et al. 2001) and characterizing the contour deformation for the same 2-D object as a function of time, *e.g.*, deforming contours of the cardiac structures in 2D + T frames (Mulet-Parada and Noble 2000; Ye and Nobel 2002; Papademetris et al. 2002) or other physical variables, *e.g.*, lesion deformation caused by probe compression (Moon et al. 2005).

Boundary delineation in a sonogram, however, is generally a hard task. Manual demarcation may be the first solution but it suffers at least two deficiencies. The contours drawn by two experts, or by the same expert at different times, may diverge substantially. Moreover, for

Address correspondence to: Chung-Ming Chen, Institute of Biomedical Engineering, College of Medicine, National Taiwan University, #1, Sec. 1, Jen-Ai Road, Taipei, Taiwan. E-mail: chung@ntu.edu.tw

a series of 2-D images, the manually delineated boundaries in consecutive slices may vary abruptly, leading to the problem of interframe boundary discontinuity.

To avoid these potential deficiencies of manual delineation, many segmentation algorithms have been proposed previously to identify the object boundaries in a 2-D series. Most of these algorithms may be classified into three categories, namely knowledge-based, model-based and general approaches. The knowledge-based approaches incorporate the intrinsic shape properties of the object of interest as the prior knowledge, *e.g.*, the shapes of cardiac structures (Ye and Noble 2002; Dydenko *et al.* 2006). Because of the prior knowledge incorporated, these approaches are usually application specific.

The model-based approaches find the 2-D boundaries based on the mathematical shape models describing the common characteristics of the objects of interest or on the shape models constructed from the training data. Some notable approaches are modeling prostate shapes as deformable superellipses (Gong *et al.* 2004) and representing the object boundaries as a linear combination of the mean shape and a set of eigenshapes (Bosch *et al.* 2002; Xie *et al.* 2005). Because the model-based approaches assume implicitly that the object shapes do not vary significantly, they may not be applicable to capture irregular object boundaries.

The general approaches do not incorporate the shape information into the segmentation algorithms. Some of these approaches use the boundary obtained in the previous slice as a prior or a constraining template for the current slice. For examples, Hass *et al.* (2000) and Martin-Fernandez *et al.* (2005) use 1-D and 2-D Markov random fields (MRFs) to regularize the shape and control the smoothness of the contour points. Some other approaches utilize the correlated image properties, *e.g.*, optical flow estimates (Mikic *et al.* 1998), between adjacent slices to ensure the boundary continuity in the 2-D series. Although the general approaches can potentially be applied to different types of objects of interest, they are less robust to the noise compared with the other two categories.

All three categories of approaches are basically pixel-based approaches. That is, the search process for the desired contour is realized in a pixel-by-pixel fashion. A common problem shared by these type of approaches is that the derived boundary points may not locate on the visually perceivable edges. To capture the irregular 2-D boundaries in a series of 2-D images and to ensure that the derived boundary points are on visually perceivable edges, a novel cell-based two-region competition algorithm based on a MAP framework, called C2RC-MAP algorithm, is proposed in this study. The basic idea of the C2RC-MAP algorithm is to perform two-region competition in a cell-based fashion slice-

by-slice while using the contour of the previous slice as the reference to ensure the contour coherence between adjacent slices. The optimization process is guarded by a MAP framework. The posterior is maximized by an expectation-maximization (EM) algorithm (Dempster *et al.* 1977).

The unique feature of the C2RC-MAP algorithm lies in its cell-based notion. Although using the contour obtained in the previous slice as a reference is a common practice for segmenting a series of 2-D slices, cell-based deformation assures that the derived boundary points locate on the visually perceivable edges. Moreover, to have a high-quality cell-based deformation, a new cell-based MAP framework is formulated to integrate contour information from the previous slice and cell-based boundary information in the current slice.

MATERIALS AND METHODS

The proposed C2RC-MAP algorithm has been designed with two essential ideas, namely, cell-based two-region competition and cell-based MAP framework. For a series of 2-D images, the C2RC-MAP algorithm begins with any slice for which the object boundary is available. Suppose the object boundary of slice i_0 , called *initial slice*, is first delineated by any effective segmentation algorithm for ultrasound images. Assuming the region-of-interest (ROI) selected for the initial slice applicable to the entire series, all other slices will be processed either forward or backward consecutively from the initial slice. For the k^{th} slice ($k \neq i_0$), the ROI is first decomposed into a set of homogeneous areas, each called a cell, using the two-pass watershed transformation scheme used in Chen *et al.* (2005). The object of interest in the ROI is assumed to be constituted by one or multiple cells and the object boundary is a composition of cell boundaries. The object boundary derived from the previous slice is used as the *reference contour* to partition the cells in the k^{th} slice into bipartite regions, namely initial object-region (OR) and background-region (BR). The contour separating both initial object- and background-regions serves as the initial regional contour for the search of the desired boundary.

Starting from the initial regional contour, the object boundary of the current slice is sought by iteratively deforming the object- and background-regions based on the cell-based two-region competition mechanism. In each iteration, the object- and background-regions compete the cells along the boundary in-between both regions, called *regional contour*. Constrained by the reference contour, the cell-based two-region competition is guided by a cell-based MAP framework maximized by an EM algorithm iteratively. As the iterative process converges, the final regional contour defines the object

boundary and the final object-region corresponds to the object of interest in the current slice. The kernel tasks in the C2RC-MAP algorithm are described in the following, including cell generation, cell-based two-region competition, MAP framework, and EM algorithm.

Cell generation and two-pass watershed transformation

The basic deformation unit in the proposed method is a cell, which is a homogeneous area defined by the two-pass watershed transformation (Chen et al. 2005). Two passes are involved in generating the cells. In the first pass, the gradient map of an ROI is tessellated by the immersion method (Vincent and Soille 1991). The catchment basins identified in the first pass are denominated as elementary cells. To eliminate the inferior watersheds, *i.e.*, watersheds with very small gradients, the edge strengths less than $T_2 = \mu_e - \sigma_e$ are set to T_2 in the second-pass watershed transformation. The μ_e and σ_e are the mean and standard deviation of the edge strengths of the watersheds identified in the first pass. The catchment basins identified in the second pass are defined as cells.

Deriving the object boundary of the initial slice

The object boundary of the initial slice may be obtained by any effective segmentation algorithm for ultrasound images. Although this is not a part of C2RC-MAP algorithm, the algorithm used in this work to attain the object boundary of the initial slice is briefly described below because of the limited space, the details of which may be found in Chen et al. (2006). The cell competition algorithm (Chen et al. 2005) is first applied to the ROI of the initial slice to find all prominent components in the ROI. A “prominent component” is a contiguous region that has a visually perceivable boundary enclosing a largely homogeneous area. Because it is common to have more than one prominent component in an object of interest, a cell-based graph-searching algorithm is further used to suggest the five most likely object boundaries to be selected by the medical doctors.

Unlike the conventional pixel-based approaches, the cell-based graph-searching algorithm regards the results derived by the cell competition algorithm as a graph, called a c-graph. In a c-graph, each node corresponds to an edge shared by two cells and two nodes are connected by a link if the edges associated with these two nodes intersect with each other. Five best object boundaries are derived by traversing the c-graph with five different cost functions optimized, which are overall absolute difference of bilateral mean gray levels, continuity of mean gradient, overall edge strength, continuity of mean gray levels and sum of the continuity of mean gray levels and the negative overall edge strength. It is assumed that either the mean gray level of the outer area is greater than that of the inner area for every boundary segment along

the path, or the former is smaller than the latter for every boundary segment along the path. A boundary segment is a small portion of a boundary uniquely shared by two elementary cells residing within two different regions. To limit the search space for the optimal solutions, we use the region competition algorithm (Zhu and Yuille 1996) to derive a rough boundary consisting of some portions of the desired boundary. By evaluating the edges commonly found by both cell and region competition algorithms, we are able to guess some boundary segments probably on the object boundary, which are then used as constraints for graph traversing. The region competition algorithm may be replaced by any other segmentation algorithm as long as this algorithm provides a rough solution comprising some parts of the desirable boundary.

Cell-based two-region competition

With the object boundary of the initial slice, all other slices in the series will be processed based on the cell-based two-region competition mechanism, which deforms the regional contour in a cell-by-cell manner. The object- and background-regions complete the cells along the regional contour and move the cell that results in the maximal improvement of the cost function in each iteration. The cell-based deformation not only guarantees that the derived boundary be on the visually perceivable edges but also that it tends to be more robust to the isolated noises than the pixel-based deformation (Chen et al. 2005).

The cell-based two-region competition process is governed by a MAP framework. Let I and C denote the set of mean gray levels of the cells in the ROI of the current slice and the regional contour separating the object-and background-regions, respectively. Denote ξ_i the i^{th} cell in the ROI. Define $L = (l_1, l_2, \dots, l_n)$ the labeling vector of the cells in the ROI, where $l_i \in \{\text{OR}, \text{BR}\}$, $1 \leq i \leq n$, denoting the labeling of ξ_i and n is the number of cells in the ROI. The posterior to be maximized, denoted as $p(L, C | I)$, is the conditional joint probability of the bipartite cell labeling and the regional contour given the ROI. The derived object boundary of the previous slice is used as a reference contour in generating the initial regional contour and in the cell-based two-region competition process. The initial regional contour is defined as the closed contour on the cell boundaries closest to the reference contour.

According to the Bayes' rule, the posterior $p(L, C | I)$ may be written as:

$$p(L, C | I) = p(I | L, C)p(C | L)p(L)/p(I) \quad (1)$$

The first term $p(I | L, C)$ may be interpreted as the region

appearance probability model, which describes the conditional joint probability of the mean gray levels of the cells in both regions. The second term $p(C|L)$ is the contour model characterizing the salience of the regional contour and the coherence of the regional contour to the reference contour. The third term $p(L)$ is the prior model for the labeling of the cells. Since $p(I)$ may be regarded as a constant given an ROI, it can be neglected in the maximization process.

Region appearance probability model

Let μ_i denote the mean gray level of cell i . Conditioned on L and C , the mean gray level of a cell is assumed to be distributed normally, *i.e.*, $p(\mu_i|L, C) \sim N(\mu_i; \mu_i, \sigma_i^2)$, where $l_i \in \{\text{OR}, \text{BR}\}$, $1 \leq i \leq n$, denoting the labeling of cell i , and μ_{l_i} and $\sigma_{l_i}^2$ are the mean and variance of the mean gray levels of the cells with the same label l_i . The region appearance probability model is thus defined as

$$p(I|L, C) = \prod_{i=1}^n p(\mu_i|L, C), \quad (2)$$

which quantifies the likelihood of a clustering that partitions the cells into two given regions.

Contour model

Let C_L be the regional contour given a cell labeling L and $\phi_L = \{b_1, b_2, \dots, b_{N_L}\}$ be the set of boundary segments on C_L , where b_j is the j^{th} boundary segment and N_L the number of boundary segments in ϕ_L . The statistical significance of b_j being an edge is defined as the minimum of three p -values derived by three two-tailed Kolmogorov-Smirnov (KS) tests, respectively. The first KS test evaluates the similarity between the gray-level distributions of the two elementary cells sharing b_j . Let e_{j1} and e_{j2} denote these two elementary cells and Λ_j denote the 15-pixel-wide band along b_j . That is, the banding area on each side of b_j is 7 pixels wide. The other two KS tests are to assess the similarity between the gray-level distributions of Λ_j and e_{j1} , as well as Λ_j and e_{j2} , respectively. Let p_j be the minimum of the p -values derived in these three KS tests. The probability that b_j is an edge is defined as $(1 - p_j)$. The salience of C_L is then defined as

$$\aleph_L = \prod_{\forall b_j \in \phi_L} (1 - p_j), \quad (3)$$

which is a conditional joint probability that measures the overall significance of all boundary segments in C_L given the cell labeling L .

The coherence of C_L to the reference contour, denoted as ρ_L is a measure that quantifies the closeness of

C_L to the reference contour given the cell labeling L . Denote λ the reference contour and $\{\lambda_1, \lambda_2, \dots, \lambda_{N_\lambda}\}$ the set of points in the contour. Suppose C_L is composed of a set of cell edges, namely, $\{a_1, a_2, \dots, a_{N_{ce}}\}$, where a cell edge is an edge shared by two cells. Furthermore, suppose a_j consists of N_j points, namely, $\{\omega_1, \omega_2, \dots, \omega_{N_j}\}$. The distance from C_L to λ , denoted as D_L , is then defined as

$$D_L = \frac{1}{N_{ce}} \sum_{j=1}^{N_{ce}} \frac{1}{N_j} \sum_{\forall \omega_q \in a_j} d_0(\omega_q, \lambda) \quad (4)$$

where $d_0(\omega_q, \lambda)$ is the minimum of the Euclidean distances from ω_q to every point λ_k in the reference contour λ . The coherence of C_L to λ is thus defined as

$$\rho_L = \kappa \exp\{-\kappa D_L\} \quad (5)$$

and

$$\kappa = \frac{\sum_{\forall b_j \in \phi_{L_0}} \ln(1 - p_j)}{D_{L_0}}, \quad (6)$$

where the subscript L_0 indicates the initial cell labeling. Combining the salience of the regional contour and the coherence of the regional contour to the reference contour given an instance of the cell labeling, the contour model is defined as

$$p(C|L) = \aleph_L \cdot \rho_L = \kappa \prod_{\forall b_j \in \phi_L} (1 - p_j) \cdot \exp(-\kappa D_L). \quad (7)$$

Prior

The labeling of each cell may be modeled as a MRF depending only on the labeling of the neighboring cells. According to the Hammersley-Clifford Theorem, an MRF cell labeling may be modeled as a Gibbs distribution, *i.e.*,

$$p(L) = Z^{-1} \exp\{-U(L)\} \quad (8)$$

where Z is a normalization constant. $U(L)$ is the energy function defined as

$$U(L) = \frac{1}{2} \sum_{\forall \xi_i} \sum_{\forall c_{ij} \in \Theta} V_{c_{ij}}(l_i) \quad (9)$$

where Θ denotes the set of all adjacent pairs of cells, $V_{c_{ij}}(l_i) = 1 - \delta_{ij}$, and

$$\delta_{ij} = \begin{cases} 1, & \text{if } l_i = l_j \\ 0, & \text{otherwise.} \end{cases} \quad (10)$$

Generally speaking, the prior prefers a smooth boundary to a protruding one.

EM algorithm

The optimal regional contour is sought by maximizing the logarithm of the posterior function by using the EM algorithm (Dempster et al. 1977). The logarithm of the posterior may be expressed as

$$\begin{aligned} \ln p(L, C | I) &= \ln p(I | L, C) + \ln p(C | L) + \ln p(L) \\ -\ln p(I) &= -\sum_{i=1}^n \frac{(\mu_i - \mu_{i_i})^2}{2\sigma_{i_i}^2} + \sum_{\forall b_j \in \phi_L} \ln(1 - p_j) - \kappa D_L \\ &\quad - \frac{1}{2} \sum_{\forall \xi_i} \sum_{\forall c_{ij} \in \Theta} V_{c_{ij}}(I_i) + K_a \quad (11) \end{aligned}$$

where \ln is the natural logarithm and K_a is a constant term absorbing all additive constants in the log-posterior. In the E-step, given the μ_{OR} , σ_{OR}^2 , μ_{BR} and σ_{BR}^2 derived in the M-step of the previous iteration, the cell-based two-region competition process is performed to find the single-cell migration from one region to the other that results in the largest positive increment of the log-posterior. In the M-step, given the new cell labeling and the new regional contour, the μ_{OR} , σ_{OR}^2 , μ_{BR} and σ_{BR}^2 are re-computed and to be used by the E-step of the next iteration. The E-step and M-step iterate until no more cell migration can cause positive increment of log-posterior. As the EM algorithm converges, the final regional contour is considered as the derived object boundary of the current slice and it will be used as the reference contour for the next slice.

Performance analysis

The performance of the proposed C2RC-MAP algorithm is evaluated based on 10 sets of serial breast sonograms, including seven sets of compression series and three sets of freehand transversal acquisition. The compression series are composed of two carcinoma cases and five fibroadenoma cases. The freehand series are composed of two carcinoma cases and one fibroadenoma case. The lesion sizes range from 0.9 cm to 1.8 cm with the mean of 1.4 cm. All images were directly stored (using the system built-in function) in an HDI 5000 US imaging system (Philips Medical Systems), equipped with a broadband L12-5 linear electronically focused transducer with cine-loop capability. Each series consists of 20 images, selected from a cine loop with every two consecutive selected images at least 10 frames apart and visible shape difference between the lesions in the selected images. The Institutional Review Boards agreed that the patients' images could be used for study without written consent if the patients' privacy could be well protected. This regulation has been carefully followed in this study.

Because the true object boundaries are generally

unknown in the clinical ultrasound images, the boundaries derived by the C2RC-MAP algorithm are compared with the manually delineated boundaries. To account for the potential variation inherent in manual delineation, the object boundary of each slice is demarcated by four graduate students supervised and approved by four medical doctors, respectively. Furthermore, to evaluate the robustness of the C2RC-MAP algorithm to the variation of the ROI, four different ROIs covering the object of interest are generated to derive four sets of object boundaries for each series of 2-D slices. The centers of these four ROIs are determined by adding random offsets, ranging from 5 to 20 pixels, in the directions of 0°, 90°, 180° and 270°, relative to a specified point, respectively. That is, each slice would have four different computer-generated boundaries.

Denote C_{ij}^s the j^{th} computer-generated boundary for the q^{th} image in the s^{th} series, derived by using the j^{th} ROI, where $1 \leq j \leq 4$ and $1 \leq q \leq 20$. Denote O_i^s the boundary delineated by observer i for the q^{th} image in the s^{th} series. Four assessments are carried out to evaluate the quality of the computer-generated boundaries based on the manually delineated boundaries. To reduce the potential bias as a result of the limited number of slices in a series and the lesion-dependent boundary characteristic, these four assessments are performed based on a series group, *i.e.*, the compression series group and the freehand series group. Both groups tend to have different types of difficulties for boundary delineation. A freehand series is inclined to have a larger variation in the 2-D lesion shape, whereas the lesions in a compression series usually have a more significant spatial shift between consecutive slices.

The first assessment is to check if the computer-to-observer distance is less than the maximum interobserver distance, both of which are calculated relative to the same manually delineated boundary. A computer-to-observer distance is the distance between a computer-generated boundary and the boundary delineated by an observer. For the q^{th} image in the s^{th} series, the maximum interobserver distance relative to the boundary delineated by observer i is defined as

$$r_{qi}^s = \max_j \{e(O_{qi}^s, O_{ij}^s) \mid 1 \leq j \leq 4, j \neq i\} \quad (12)$$

where $e(A, B)$ is the distance between contours A and B , which is defined as the average of the minimum distances from each point of these two contours to the other contour.

For the j^{th} set of computer-generated boundaries of a series group, two performance indices are reported. One performance index is the percentage, denoted by P_{ij} , of the computer-generated boundaries that have smaller computer-to-observer distances than the corresponding

maximum interobserver distances relative to the boundaries delineated by observer i . The other performance index is the mean of the differences, denoted by k_{ij} , between the computer-to-observer distances and the corresponding maximum interobserver distances relative to the boundaries delineated by observer i , which is defined as

$$k_{ij} = \frac{1}{N \cdot N_{\Omega}} \sum_{\forall s \in \Omega} \sum_{q=1}^{20} (e(C_{qj}^s, C_{qi}^s) - r_{qi}^s), \quad (13)$$

where Ω and N_{Ω} represent the series group and the number of series in the group. To test if $k_{ij} < 0$, the 95% confidence interval for the statistic k_{ij} is computed to check if the upper bound of the confidence interval is less than zero.

The second assessment tests if there is a significant difference among the four sets of computer-generated boundaries of a series group with respect to the average manually delineated boundaries. Denote O^s the average manually delineated boundary for the q^{th} image in the s^{th} series. Let $S_j = \{e(C_{qj}^s, C_q^s) \mid 1 \leq q \leq 20, 1 \leq s \leq N_{\Omega}\}$, $1 \leq j \leq 4$, represent the set of distances between the j^{th} set of computer-generated boundaries and the corresponding average manually delineated boundaries for a series group. Friedman test for related samples (Daniel 1978) is used to test if there is a significant difference among four S_j , $1 \leq j \leq 4$.

The third assessment is to check if the lesion sizes enclosed by the j^{th} set of computer-generated boundaries j , $1 \leq j \leq 4$, are closely correlated with those enclosed by the corresponding average manually delineated boundaries for each series group. Let $X_j = \{x_{qi}^s \mid 1 \leq q \leq 20, 1 \leq s \leq N_{\Omega}\}$, and $Y = \{y_q^s \mid 1 \leq q \leq 20, 1 \leq s \leq N_{\Omega}\}$, where x_{qi}^s and y_q^s denote the lesion sizes enclosed by C_{qj}^s and O_q^s , respectively, for the q^{th} image in the s^{th} series of the series group Ω . The third assessment computes the Pearson's correlation of X_j and Y for each j , $1 \leq j \leq 4$.

The fourth assessment evaluates how well the regions defined by the computer-generated boundaries match those defined by the average manually delineated boundaries. Two metrics are used to quantify the degree of matching between a computer-generated boundary, C_{qj}^s , and the corresponding average manually delineated boundary, O_q^s . One is the overlapping ratio, which is defined as the ratio of the size of the overlapped region of C_{qj}^s and O_q^s to y_q^s . The other is difference ratio, which is defined as the ratio of the size of the difference region of C_{qj}^s and O_q^s to y_q^s . The difference region is the region enclosed by either C_{qj}^s or O_q^s , but not both. The fourth assessment reports the overall degree of matching between the j^{th} set of computer-generated boundaries, $1 \leq j \leq 4$, and the corresponding set of average manually

delineated boundaries of the same series group. The overall degree of matching is quantified by the (mean \pm standard deviation)'s of the overlapping ratios and the difference ratios, respectively.

To compare with the conventional approaches, the level set method proposed by Chan and Vese (2001) is evaluated by the same four assessments as for the proposed C2RC-MAP algorithm using the 10 series groups. The level set method is chosen for comparison mainly because it is a general approach and it has been employed in segmentation of sonographic breast lesions (Chang *et al.* 2005; Shreedhara and Kumar 2005). This level set method is modified in such a way that the lesion boundary derived for the previous slice is used as the initial contour of the current slice.

To compare the performances of the proposed C2RC-MAP algorithm and the level set method proposed by Chan and Vese (2001), four one-tailed paired-sample t -tests are carried out for each series group. These four paired-sample t -tests test if the means of the mean P_{ij} 's, the Pearson's correlations, the mean overlapping ratios and the mean difference ratios achieved by the proposed algorithm are better than those achieved by the Chan and Vese level set method. The significance level for each paired-sample t -test is set to 5%.

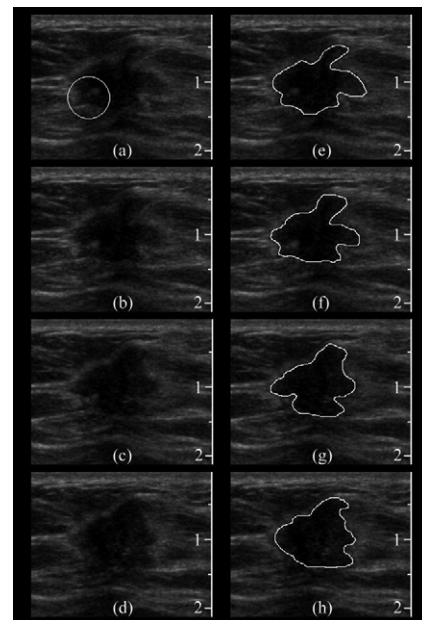


Fig. 1. (a–d) The lesion clips in four consecutive slices in a freehand series. (e–h) Manually delineated boundaries for these four clips, in which incoherent lesion boundaries may be observed at the lower left part of (f) and (g). The scale bar at the right side of each clip shows the depth and scale of the clip, in which the distance between two consecutive markers (“-”) is 0.5 cm.

RESULTS AND DISCUSSION

To demonstrate the potential coherence problem, Fig. 1a–d shows the lesion clips in four consecutive slices in a freehand series. The coherence problem might occur at the lower-left part of the lesion as indicated by a white circle in Fig. 1a, in which a small structure can be clearly observed in the first three clips. Although it is not clear what the small structure is and where its true edge is without rigorous verification, it is reasonable to assume that the lesion either includes the small structure or excludes it, but not both. If one does not make a reference to the second clip when delineating the lesion boundary of the third one, it is likely that the small structure is included in the lesion in some slices but excluded in others. Figure 1e–h gives one such manual demarcation for these four clips, in which incoherent lesion boundaries may be observed at the lower left part of Fig. 1f and g. On the other hand, the common deficiencies of most conventional segmentation algorithms are exemplified in Fig. 2a–d, where the lesion boundaries of these four clips are derived by using the Chan and Vese level set method. Although not so serious as the manual delineation demonstrated in Fig. 1e–h, the boundary incoherence between consecutive slices can still be observed at the lower left part of the lesions in Fig. 2a–d. Moreover, it is obvious that the derived boundaries do not follow the visually perceivable lesion

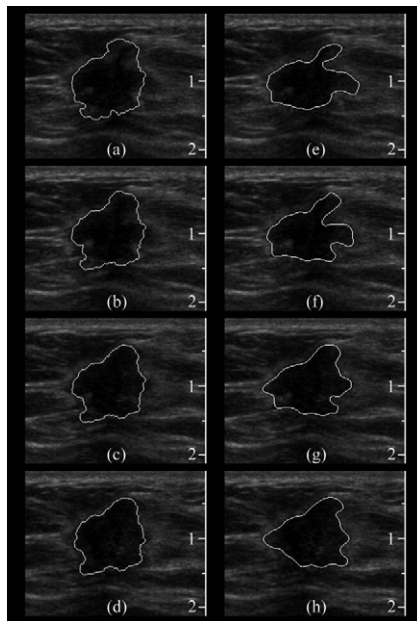


Fig. 2. (a–d) The lesion boundaries derived by using the Chan and Vese level set method for the four clips given in Fig. 1. (e–h) The boundaries derived by the proposed C2RC-MAP algorithm. The scale bar at the right side of each clip shows the depth and scale of the clip, in which the distance between two consecutive markers (“-”) is 0.5 cm.

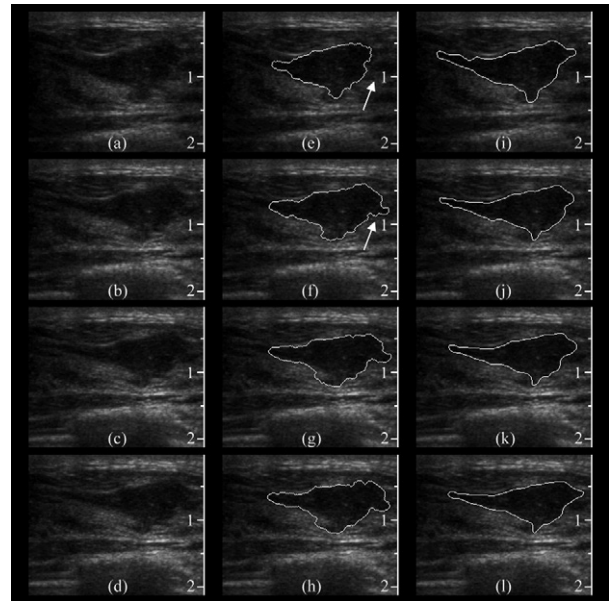


Fig. 3. (a–d) The lesion clips in four consecutive slices in a compression series. (e–h) The boundaries derived by the Chan and Vese level set method. (i–l) The boundaries derived by the C2RC-MAP algorithm. The scale bar at the right side of each clip shows the depth and scale of the clip, in which the distance between two consecutive markers (“-”) is 0.5 cm.

boundaries closely, which is a common phenomenon for the pixel-based segmentation algorithms, especially for a low-contrast boundary.

The lesion boundaries derived by using the proposed C2RC-MAP algorithm are displayed in Fig. 2e–h. Noticeably, a coherent delineation has been achieved at the lower left part, which may be attributed to the regularization effect exerted by the ρ_L term in the contour model. Furthermore, the derived boundaries follow the visually perceivable edges much better than those in Fig. 2a–d because of the cell-based deformation, which promises that all edges in a derived boundary are visually perceivable edges.

As another example, Fig. 3a–d shows four consecutive slices of a compression series. Figure 3e–h and i–l give the boundaries derived by the Chan and Vese level set method and the C2RC-MAP algorithm, respectively. Like in a freehand series, the boundaries identified by the C2RC-MAP algorithm not only have better boundary coherence but also follow the visually perceivable boundaries more closely than those obtained by the Chan and Vese level set method. In particular, boundary incoherence can be observed between the first and second slices in the boundaries derived by the Chan and Vese level set method as indicated by the white arrows.

The null hypothesis for the first assessment is $k_{ij} \geq 0$ and the significance level is set to 0.05. As examples, Table 1 shows k_{ij} , 95% confidence interval for k_{ij} and P_{ij}

Table 1. The mean computer-to-observer distances versus mean maximum interobserver distances for the first set of computer-generated boundaries of the compression and freehand series groups (all distances in pixels) achieved by the proposed C2RC-MAP algorithm

Observer i	Compression series group			Freehand series group		
	k_{ij}	95% CI	P_{i1}	k_{ij}	95% CI	P_{i1}
1	-1.25	(-1.42, -1.08)	92.86%	-0.87	(-1.09, -0.64)	86.67%
2	-1.05	(-1.19, -0.91)	87.14%	-0.45	(-0.64, -0.27)	73.33%
3	-0.65	(-0.75, -0.55)	90.71%	-0.52	(-0.69, -0.36)	85.00%
4	-0.71	(-0.84, -0.59)	84.29%	-0.58	(-0.73, -0.44)	86.67%

for the first set of computer-generated boundaries of the compression and freehand series groups achieved by the proposed C2RC-MAP algorithm, respectively. Note that the upper bounds of the 95% confidence intervals are less than 0 for all observers in Table 1, which suggests that the null hypothesis is rejected for the first set of computer-generated boundaries for both series groups. Although not listed, the same conclusions may be drawn for all of the other sets of computer-generated boundaries. That is, for both compression and freehand series groups, the proposed C2RC-MAP algorithm is capable of delineating the boundaries with a smaller mean computer-to-observer distance than the mean maximum interobserver distance at a 5% significance level.

From P_{ij} 's in Table 1, one may see that the computer-to-observer distances for most slices fall within the interobserver ranges for both series groups. Table 2 further summarizes the means and standard deviations of the statistic P_{ij} , with respect to each observer i for the four sets of computer-generated boundaries derived for the compression and freehand series groups by the proposed C2RC-MAP algorithm. Evidently, for both series groups, at least 70% (mostly >80%) of computer-generated boundaries delineated by the proposed algorithm achieve the computer-to-observer distances that are smaller than the maximum interobserver ranges. Moreover, the percentages tend to be higher for the compression series group than for the freehand series group. The first assessment assures that the boundaries derived by the C2RC-MAP algorithm fall within the span of the reasonable boundaries defined by the manually delineated boundaries.

The null hypothesis for the second assessment is that there is no difference among S_j , $1 \leq j \leq 4$, for each series group. The p -values of the Friedman tests for the compression and freehand series groups are 0.517 and 0.352, respectively. It suggests that the null hypotheses are accepted for both series groups, *i.e.*, there is no difference among S_j , $1 \leq j \leq 4$, for each series group at a 5% significance level.

For the third assessment, the Pearson's correlations for the four sets of computer-generated boundaries are

0.995, 0.995, 0.994 and 0.995 for the compression series group. The four Pearson's correlations are 0.992, 0.994, 0.994 and 0.993 for the freehand series group. The high Pearson's correlations suggest that the lesion sizes derived by the proposed C2RC-MAP algorithm are highly correlated with the lesions defined by the average manually delineated boundaries.

The results of the fourth assessment are summarized in Table 3, which shows the (mean \pm standard deviation)'s of the overlapping ratios and the difference ratios for the compression and freehand series groups for all four sets of computer-generated boundaries. Both ratios suggest that the computer-generated boundaries match the average manually delineated boundaries reasonably well. For most computer-generated boundaries, the overlapping ratio is higher than 0.90 and the difference ratio is lower than 0.13.

All four assessments have corroborated that the lesion boundaries derived by the proposed algorithm are comparable to those demarcated manually for both of the compression and freehand series groups. Furthermore, the robustness of the proposed algorithm to the variation of the ROIs has been partially validated by using four different ROIs for each series.

For comparative performance analysis, the same four assessments as the proposed algorithm are performed for the level set method proposed by Chan and Vese (2001). For the first assessment, the analysis results show that the lower bounds of the 95% confidence intervals of k_{ij} 's are greater than 0 for all $1 \leq i \leq 4$ and

Table 2. The means and standard deviations of the statistic P_{ij} with respect to each observer i for the four sets of computer-generated boundaries derived for the compression and freehand series groups by the proposed C2RC-MAP algorithm

Observer i	Compression (%)	Freehand (%)
1	(95.00 \pm 1.75)	(88.75 \pm 2.10)
2	(89.46 \pm 2.70)	(74.17 \pm 2.15)
3	(92.14 \pm 1.31)	(83.33 \pm 1.36)
4	(86.61 \pm 1.97)	(84.59 \pm 2.50)

Table 3. The means and standard deviations of the overlapping ratios and the difference ratios for the compression and freehand series groups for all four sets of computer-generated boundaries derived by the proposed C2RC-MAP algorithm

Computer-generated boundaries	Compression		Freehand	
	Overlapping	Difference	Overlapping	Difference
1	(0.950 ± 0.017)	(0.069 ± 0.019)	(0.937 ± 0.026)	(0.093 ± 0.033)
2	(0.952 ± 0.017)	(0.066 ± 0.018)	(0.933 ± 0.031)	(0.092 ± 0.034)
3	(0.949 ± 0.018)	(0.067 ± 0.020)	(0.934 ± 0.028)	(0.093 ± 0.033)
4	(0.951 ± 0.016)	(0.068 ± 0.019)	(0.941 ± 0.026)	(0.092 ± 0.035)

$1 \leq j \leq 4$ for both of the compression and freehand series groups. We may conclude that for both compression and freehand series groups, the mean computer-to-observer distance attained by the Chan and Vese level set method is greater than the corresponding mean maximum interobserver distance at a 5% significance level. As examples, Table 4 shows k_{ij} , 95% confidence interval for k_{ij} and P_{ij} for the first set of computer-generated boundaries of the compression and freehand series groups achieved by the Chan and Vese level set method, respectively. Note that all lower bounds of the 95% confidence intervals in Table 4 are greater than 0. Furthermore, Table 5 summarizes the means and standard deviations of the statistic P_{ij} for the compression and freehand series groups achieved by the Chan and Vese level set method, which clearly shows that the computer-to-observer distances are greater than the corresponding maximum interobserver distances for most slices. In comparing the mean P_{ij} 's achieved by the proposed algorithm and the Chan and Vese level set method, the p -values for these two paired-sample t -tests are 0.000 and 0.000 for the compression and freehand series groups, respectively. Because both p -values are < 0.05 , we may conclude that the means of the mean P_{ij} 's achieved by the proposed algorithm are larger than those achieved by the Chan and Vese level set method at a 5% significance level for both series groups.

For the second assessment, the p -values of the Friedman tests for the compression and freehand series groups are $1.2e-5$ and $1e-4$, respectively, which means there exists significant difference among S_j , $1 \leq j \leq 4$, for each series group at 5% significance level. For the third assessment, the four Pearson's correlations for the compression series group are 0.992, 0.938, 0.969 and 0.939, and those for the freehand series group are 0.987, 0.990, 0.991 and 0.980. In the comparisons of the Pearson's correlations achieved by both algorithms for each series group, the p -values for the paired-sample t -tests are 0.037 and 0.036 for the compression and freehand series groups, respectively. Because both p -values are < 0.05 , we may conclude that the means of the Pearson's correlations achieved by the proposed algorithm are larger than those achieved by the Chan and Vese level set method at a 5% significance level for both series groups.

The results of the fourth assessment are summarized in Table 6, which shows the (mean ± standard deviation)'s of the overlapping ratios and the difference ratios for the compression and freehand series groups for all four sets of computer-generated boundaries. For most computer-generated boundaries, the overlapping ratio is higher than 0.80 and the difference ratio is lower than 0.27. One-tailed paired-sample t -tests are carried out to compare the means of the overlapping ratios and the difference ratios achieved by the proposed algorithm and the Chan and Vese level set method for each series group. Consequently, the p -values for the overlapping

Table 4. The mean computer-to-observer distances versus mean maximum interobserver distances for the first set of computer-generated boundaries of the compression and freehand series groups (all distances in pixels) achieved by the Chan and Vese level set method

Observer i	Compression series group			Freehand series group		
	k_{ij}	95% CI	P_{i1}	k_{ij}	95% CI	P_{i1}
1	1.48	(1.14, 1.84)	25.00%	1.37	(0.85, 1.91)	30.00%
2	1.64	(1.27, 2.02)	27.14%	1.57	(1.23, 1.91)	10.00%
3	1.52	(1.17, 1.89)	25.00%	1.78	(1.38, 2.17)	11.67%
4	1.43	(1.11, 1.75)	27.14%	1.45	(0.97, 1.93)	33.33%

Table 5. The means and standard deviations of the statistic P_{ij} with respect to each observer i for the four sets of computer-generated boundaries derived for the compression and freehand series groups by the Chan and Vese level set method

Observer i	Compression (%)	Freehand (%)
1	(27.14 ± 1.75)	(32.92 ± 2.10)
2	(28.93 ± 3.00)	(14.17 ± 6.74)
3	(22.32 ± 4.45)	(17.09 ± 4.17)
4	(22.86 ± 3.82)	(35.42 ± 1.60)

Table 6. The means and standard deviations of the overlapping ratios and the difference ratios for the compression and freehand series groups for all four sets of computer-generated boundaries derived by the Chan and Vese level set method

Computer-generated boundaries	Compression		Freehand	
	Overlapping	Difference	Overlapping	Difference
1	(0.938 ± 0.028)	(0.147 ± 0.051)	(0.878 ± 0.092)	(0.188 ± 0.083)
2	(0.922 ± 0.048)	(0.158 ± 0.057)	(0.901 ± 0.047)	(0.171 ± 0.081)
3	(0.925 ± 0.028)	(0.147 ± 0.047)	(0.907 ± 0.041)	(0.180 ± 0.083)
4	(0.925 ± 0.027)	(0.148 ± 0.053)	(0.917 ± 0.042)	(0.184 ± 0.078)

ratios are 0.005 and 0.01, and those for the difference ratios are 0.000 and 0.000 for the compression and freehand series groups, respectively. We may thus conclude that the means of the overlapping ratios and the difference ratios achieved by the proposed algorithm are better than those achieved by the Chan and Vese level set method at a 5% significance level.

Based on the results of the paired-sample *t*-tests on different performance indices, it is clear that the proposed C2RC-MAP algorithm is superior to the level set method proposed by Chan and Vese (2001) for both series groups. The superiority of the C2RC-MAP algorithm comes mainly from the cell-based two-region competition and cell-based MAP framework. While the former ensures that the derived boundaries closely follow the visually perceivable edges, the latter enforces the boundary coherence between consecutive slices. On the other hand, the inferior performance of the Chan and Vese level set method may be ascribed to its two inherent properties. One is the pixel-based deformation and the other is the two region-based terms in the energy function. The pixel-based deformation makes the level set function easily trapped in a local minimum that may not locate on the visually perceivable edges. The two region-based terms quantify the sums of the squared differences within the inner and outer regions defined by the level set function. For a lesion with the heterogeneous inner and outer regions, a boundary minimizing the energy function, particularly balancing the two region-based terms, does not necessarily coincide with the visually perceivable edges, which may be easily observed in Fig. 2a–d. Figure 4a and b further shows the boundaries (white contours) derived by the Chan and Vese level set method and the proposed algorithm, respectively, superimposed on the four manually delineated boundaries (color contours in dark orange, dark violet, royal blue and lime green) for Fig. 1b. The boundary defined by the proposed algorithm clearly matches the manually delineated boundaries better than the boundary defined by the Chan and Vese level set method.

CONCLUSIONS

To ensure the derived boundaries locating on the visually perceivable edges and to preserve the boundary coherence between consecutive slices, a nearly automatic cell-based two-region competition algorithm based on a MAP framework is proposed in this paper for boundary delineation of a series of 2-D sonograms. The unique feature of the proposed C2RC-MAP algorithm lies in its cell-based notion in the deformation of the regional contour and in the construction of the MAP framework. The C2RC-MAP algorithm deforms the regional contour in a cell-by-cell fashion through a cell-based two-region competition process. It not only promises that the derived boundaries locate on the visually perceivable edges, but also offers a better opportunity to find the optimum regional contour. The cell-based MAP framework further guides the cell-based deformation of the regional contour with the region appearance probability model, contour model and prior model.

The performance of the proposed C2RC-MAP algorithm has been validated by using 10 series of breast sonograms, including seven compression series and three freehand series. Using the manually delineated lesion boundaries as the basis of the performance analysis, four assessments have been carried out to evaluate the quality of the derived boundaries. The first assessment confirms

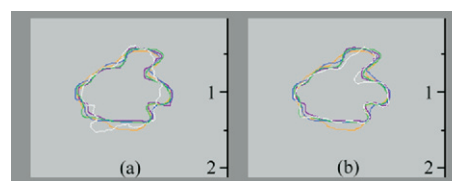


Fig. 4. The boundaries (white contours) derived by (a) the Chan and Vese level set method, and (b) the C2RC-MAP algorithm, respectively, both superimposed on the four manually delineated boundaries (color contours in dark orange, dark violet, royal blue and lime green) for Fig. 1. (b) The scale bar at the right side of each clip shows the depth and scale of the clip, in which the distance between two consecutive markers (“-”) is 0.5 cm.

that more than 70% of derived boundaries achieve the computer-to-observer distances smaller than the maximum interobserver distances for both series groups. The second assessment corroborates the robustness of the proposed algorithm to the variation of ROI by using the Friedman tests, the p -values of which are 0.517 and 0.352 for the compression and freehand series groups, respectively. The third assessment shows that the lesion sizes derived by the proposed algorithm are highly correlated with those defined by the average manually delineated boundaries. All Pearson's correlations computed are higher than 0.990. The fourth assessment shows that for most computer-generated boundaries, the overlapping ratio is higher than 0.90 and the difference ratio is lower than 0.13. For both series groups, all four assessments conclude that the object boundaries attained by the proposed C2RC-MAP algorithm be comparable to those delineated manually.

In comparison with the conventional approaches, the level set method proposed by Chan and Vese (2001) has been evaluated by the same four assessments. Based on the paired-sample-tests on the performance indices computed in the first, third and fourth assessments, it is shown that the proposed C2RC-MAP algorithm is superior to the Chan and Vese level set method at a 5% significance level.

Acknowledgements—This work was supported by National Science Council, Taiwan, R.O.C., under the grant numbers NSC94-2622-E-002-002- and NSC95-2221-E-002-023-MY3.

REFERENCES

- Bosch JG, Mitchell SC, Lelieveldt BPF, Nijland F, Kamp O, Sonka M, Reiber JHC. Automatic asegmentation of cchocardiographic sequences by active appearance motion models. *IEEE Trans Med Imaging* 2002;21(11):1374–1383.
- Chan TF, Vese LA. Active contours without edges. *IEEE Trans Image Proc* 2001;10(2):266–277.
- Chang RF, Wu WJ, Moon WK, Chen DR. Automatic ultrasound segmentation and morphology based diagnosis of solid breast tumors. *Breast Cancer Res Treatment* 2005;89:179–185.
- Chen CM, Chou YH, Chen CSK, Cheng JZ, Ou YF, Yeh FC, Chen KW. Cell-competition algorithm: A new segmentation algorithm for multiple objects with irregular boundaries in ultrasound images. *Ultrasound Med Biol* 2005;31(12):1647–1664.
- Chen CM, Cheng JZ, Chou YH. ACCOMP—Augmented cell competition algorithm for delineating boundaries of objects of interested in sonography. Technical Report: IBME-TR-20061101, <http://www.csie.ntu.edu.tw/~b7506034/TR.pdf>, National Taiwan University, Taiwan, 2006.
- Chen DR, Chang RF, Wu WJ, Moon WK, Wu WL. 3D Breast ultrasound segmentation using active contour model. *Ultrasound Med Biol* 2003;29(7):1017–1026.
- Daniel WW. *Applied nonparametric statistics*. Boston, MA: Houghton Mifflin, 1978.
- Dempster AP, Laird NM, Rubin DB. Maximum likelihood from incomplete data via the EM algorithm. *J Royal Stat Soc* 1977; 39:1–38.
- Dydenko I, Jamal F, Bernard O, D'hooge J, Magnin IE, Friboulet D. A level set framework with a shape and motion prior for segmentation and region tracking in echocardiography. *Med Image Analys* 2006; 10:162–177.
- Gong L, Pathak SD, Haynor DR, Cho PS, Kim Y. Parametric shape modeling using deformable superellipses for prostate segmentation. *IEEE Trans Med Imaging* 2004;23(3):340–349.
- Hass C, Ermer H, Holt S, Grewe P, Machraoui A, Barmeyer J. Segmentation of 3D intravascular ultrasonic images based on a random field model. *Ultrasound Med Biol* 2000;26(2):297–306.
- Lee DY, Eigler N, Luo H, Nishioka T, Tabak S, Forrester JS, Siegel RJ. Effects of intracoronary ultrasound imaging on clinical decision making. *Am Heart J* 1995;129(6):1084–1093.
- Martin-Fernandez M, Alberola-Lopez C. An approach for contour detection of human kidneys for ultrasound images using Markov random fields and active contours. *Med Image Analys* 2005;9(1): 1–23.
- Mikic I, Krucinski S, Thomas JD. Segmentation and tracking in echocardiographic sequences: Active contours guided by optical flow estimates. *IEEE Trans Med Imaging* 1998;17(2):274–284.
- Moon WK, Chang RF, Chen CJ, Chen DR, Chen WL. Solid breast masses: Classification with computer-aided analysis of continuous US images obtained with probe compression. *Radiology* 2005;236: 458–464.
- Mulet-Parada M, Noble JA. 2D + T boundary detection in echocardiography. *Med Image Analys* 2000;4(1):21–30.
- Nissen SE, Yock P. Intravascular ultrasound: novel pathophysiological insights and current clinical applications. *Circulation* 2001;103(4): 604–616.
- Noble JA, Boukerroui D. Ultrasound image segmentation: A survey. *IEEE Trans Med Imaging* 2006;25(8):987–1010.
- Papademetris X, Sinusas AJ, Dione DP, Constable T, Duncan JS. Estimation of 3-D left ventricular deformation from medical images using biomechanical Models. *IEEE Trans Med Imaging* 2002; 21(7):786–800.
- Shreedhara KS, Kumar MA. 3D reconstruction of solid breast nodule in ultra sonographic image. *Proceedings of the International Conference on Cognition and Recognition* 2005;759–767.
- Vincent L, Soille P. Watershed in digital spaces: An efficient algorithm based on immersion simulations. *IEEE Trans PAMI* 1991;13(6): 583–597.
- Xie J, Jiang Y, Tsui HT. Segmentation of kidney from ultrasound images based on texture and shape priors. *IEEE Trans Med Imaging* 2005;24(1):35–57.
- Ye XJ, Noble JA. 3-D freehand echocardiography for automatic left ventricle reconstruction and analysis based on multiple acoustic windows. *IEEE Trans Med Imaging* 2002;21(9):1051–1058.
- Zhu SC, Yuille A. Region competition: Unifying snakes, region growing, and bayes/MDL for multiband image segmentation. *IEEE Trans Patt Analys Machine Intell* 1996;18(9):884–900.